# Non-Linear Aspects of a Barotropically Unstable Polar Vortex in a Forced-Dissipative System: Flow Régimes and Tracer Transport

**By Keiichi Ishioka and Shigeo Yoden**
Department of Geophysics, Kyoto University, Kyoto 606-01, Japan

*(Manuscript received 11 August 1994, in revised form 17 January 1995)*

Journal of the Meteorological Society of Japan
Vol. 73, No.2
Meteorological Society of Japan

*Journal of the Meteorological Society of Japan*, Vol. 73, No. 2, pp. 201–212, 1995



# Non-Linear Aspects of a Barotropically Unstable Polar Vortex in a Forced-Dissipative System: Flow Régimes and Tracer Transport

**By Keiichi Ishioka and Shigeo Yoden**

*Department of Geophysics, Kyoto University, Kyoto 606-01, Japan*

*(Manuscript received 11 August 1994, in revised form 17 January 1995)*

## Abstract

Non-linear dynamics of a barotropically unstable circumpolar vortex in a forced-dissipative system is investigated numerically with a high-resolution barotropic model on a spherical domain. Horizontal transport and mixing processes of a passive tracer are also investigated for several types of evolving flow fields with a high-resolution transport model.

Vacillating and irregular solutions are obtained within some parameter ranges as well as steady-wave solutions. In the vacillation, planetary waves propagate eastward, changing the horizontal structure periodically. Stepwise transitions from steady-wave solutions to irregular ones via vacillations are found for a sech-type jet which is unstable mainly on the poleward flank of the jet, while no irregular solutions are obtained for a tanh-type jet which is unstable on the equatorward flank of the jet within realistic parameter ranges of the stratosphere.

Time evolutions of an ideal passive tracer field show that the edge of the circumpolar vortex is so robust that mixing through the edge hardly occurs whether the solution is steady or not. Exceptionally intermittent intrusion and ejection of fluid through the vortex edge occur in the irregular solutions for the sech-type jet.

## 1. Introduction

Two kinds of eastward-propagating planetary waves have been observed in the southern hemisphere stratosphere during winter and spring by satellite observations. One is the wave of zonal wavenumber 2 (Wave 2) discovered by Harwood (1975) in the temperature field and by Hartmann (1976) in the geopotential height field. Wave 2 has its maximum amplitude around 50°S and the period is about 8~20 days. The other is the wave of zonal wavenumber 1 (Wave 1) discovered by Venne and Stanford (1979, 1982). Wave 1 has its maximum amplitude around 70° in both hemispheres and the period is about 4 days; thus it is sometimes called "4-day wave". Details in recent observations are summarized by Manney, Farrara and Mechoso (1991) for the Wave 2 in middle latitudes and by Manney (1991) for the Wave 1.

Since these waves are observed during winter and spring when the stratospheric polar night jet is intense, Hartmann (1983) made a linear stability analysis of an idealized polar night jet to show that barotropic instability of the polar night jet may cause the eastward-propagating waves. He obtained two kinds of unstable eigenmodes; one is associated with negative regions of latitudinal gradient of absolute vorticity on the equatorward side of the polar night jet and the other is associated with those on the poleward side of the jet. He called the former the "mid-latitude mode" and the latter the "polar mode". The period of each mode and latitude of its maximum amplitude are similar to those of the corresponding waves observed in the southern hemisphere.

After Hartmann (1983), many analyses have been done on the linear stability of the polar night jet with more realistic jet profiles (Manney, Nathan and Stanford, 1988; Manney, Mechoso, Elson and Farrara, 1991; Manney and Randel, 1993). However, there has been no study on the non-linear phase of the barotropic instability of the polar night jet, at which phase the linear unstable modes grow to have a finite amplitude and non-linear interactions become important, until that of Ishioka and Yoden (1994, hereafter referred to as IY94). They showed that dominant zonal wavenumber often decreases in

the non-linear phase of the instability from the most unstable wavenumber in the linear phase and that the absolute vorticity is mixed enough to stabilize the jet. While their results may have some implications, it is not straightforward to apply those to the real stratosphere because their model is a conserved system without any forcing or dissipation.

Tracer transport and mixing processes by the barotropically unstable waves were studied by Bowman and Chen (1994). They traced Lagrangian trajectories for large numbers of particles advected by unstable waves at finite amplitude in a non-linear shallow-water model. The main conclusion in the study is that there is little exchange of air across the vortex boundary, while the air is mixed both in middle latitudes and inside the vortex by the mid-latitude modes and polar modes, respectively. This is very interesting, because it supports the theoretical argument that strong gradients of potential vorticity are very resistant to mixing (McIntyre, 1989). However, the numerical experiments were done for some limited cases and the effect of the forcing that maintains the unstable jet was not sufficiently investigated.

Thus, in this study, we investigate the non-linear phase of the instability and the tracer transport in a more realistic situation with a forcing to maintain the unstable zonal jet and dissipation corresponding to the radiative damping. With such a forcing and dissipation, several kinds of flow régimes are expected to exist, depending on some experimental parameters as in the $\beta$-channel experiments by Kwon and Mak (1988). We sweep a parameter space which determines the prescribed jet profiles of the forcing. The model and experimental procedure are described in Section 2. Results of non-linear evolution are given in Section 3. Discussion is given in Section 4 and conclusions in Section 5.

## 2. The model

The system under consideration is non-divergent two-dimensional flow over the earth, which flow is governed by the vorticity equation in the form

$$\frac{Dq}{Dt} = -\alpha(q - \overline{q}_0) + \nu\left(\nabla^2 + \frac{2}{a^2}\right)(q - \overline{q}_0), \quad (1)$$

where $q(\lambda, \phi, t) \equiv \nabla^2\psi + 2\Omega\sin\phi$ is the absolute vorticity, $\psi(\lambda, \phi, t)$ the streamfunction, $\lambda$ the longitude, $\phi$ the latitude, $t$ the time, $a$ the radius of the earth ($= 6.37 \times 10^6$ m), $\Omega$ the angular speed of rotation of the earth ($= 7.29 \times 10^{-5}$/s), $\nabla^2$ the horizontal Laplacian:

$$\nabla^2 \equiv \frac{1}{a^2}\left[\frac{1}{\cos^2\phi}\frac{\partial^2}{\partial\lambda^2} + \frac{1}{\cos\phi}\frac{\partial}{\partial\phi}\left\{\cos\phi\frac{\partial}{\partial\phi}\right\}\right], \quad (2)$$

and $D/Dt$ the material derivative:

$$\frac{D}{Dt} \equiv \frac{\partial}{\partial t} + \frac{1}{a^2\cos\phi}\left(\frac{\partial\psi}{\partial\lambda}\frac{\partial}{\partial\phi} - \frac{\partial\psi}{\partial\phi}\frac{\partial}{\partial\lambda}\right). \quad (3)$$

The first term on the right hand side of Eq. (1) means a linear "radiative" relaxation to a zonally symmetric equilibrium state $\overline{q}_0(\phi)$, which is the absolute vorticity profile for the prescribed jet forcing defined below, and the second term is an artificial viscosity term introduced to smooth numerical behavior. Throughout this study, we fix the relaxation time as $\alpha^{-1} = 10$ days and the viscosity coefficient $\nu$ at a small constant which gives the dissipation time of 1 day at the largest total wavenumber ($N = 85$) in our model. We employ a damping rate $\alpha$ that is rather smaller than the realistic value for middle and upper stratosphere in order to examine various flow régimes which depend on the external parameters; when $\alpha$ is too large, the variety of flow régimes is limited because the damping has a stabilizing effect on the system (see, *e.g.*, Kwon and Mak, 1988).

The prescribed equilibrium state, which is barotropically unstable, is either of two types of jet profiles introduced by Hartmann (1983):

tanh-type jet:

$$\overline{u}_0(\phi) = U\cos\phi \cdot \frac{1}{2}\left(1 + \tanh\frac{\phi - \phi_0}{B}\right), \quad (4)$$

sech-type jet:

$$\overline{u}_0(\phi) = U\cos\phi \cdot \mathrm{sech}\frac{2(\phi - \phi_0)}{B}, \quad (5)$$

where $U$ is a measure of the intensity of the jet, $B$ its width, and $\phi_0$ its position. Thirty six experiments are done for each type of jet profile, changing the values of the three parameters around the values used by Hartmann (1983). Examples of the profiles of $\overline{u}_0(\phi)$ and $\overline{q}_0(\phi)$ are illustrated with dotted lines in Fig. 3 for the tanh-type jet and in Fig. 9 for the sech-type jet. The tanh-type jet has negative latitudinal gradient of zonal mean absolute vorticity on the equatorward flank of the jet axis, while for the sech-type jet it is mainly on the poleward flank of the jet axis. Note that $U$ is not representative of the actual flow speed because of the factor of $\cos\phi$ in Eqs. (4) and (5); the maximum of $\overline{u}_0(\phi)$ is about a half of $U$.

Transport and mixing processes are also investigated using a passive scalar transport model described as:

$$\frac{D\chi}{Dt} = \nu_\chi\nabla^6\chi, \quad (6)$$

where $\chi(\lambda, \phi, t)$ is a passive scalar and $\nu_\chi$ is an artificial hyper-diffusion coefficient, which is fixed at a small constant with the diffusion time-scale of 0.1 day at the largest total wavenumber ($N = 173$) in the transport model.

Equation (1) is integrated numerically for 200 days from an unstable jet profile $\overline{q}_0$ with a small disturbance, while the integration of Eq. (6) is started at a certain time of the integration period of Eq. (1) from an axisymmetric initial distribution: $\chi = \sin\phi$.

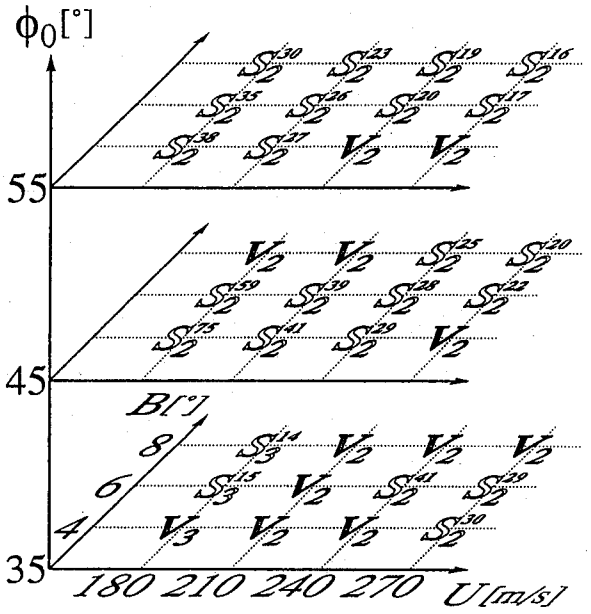


Fig. 1. Régime diagram for tanh-type jet as a function of $U$, $B$, and $\phi_0$. Symbol $S$ refers to a steady-wave solution and $V$ a vacillation. The lower suffix indicates dominant zonal wavenumber, and the upper suffix for a steady-wave solution indicates $2\pi/c$ in days, where $c$ is the angular phase velocity of the steady wave.

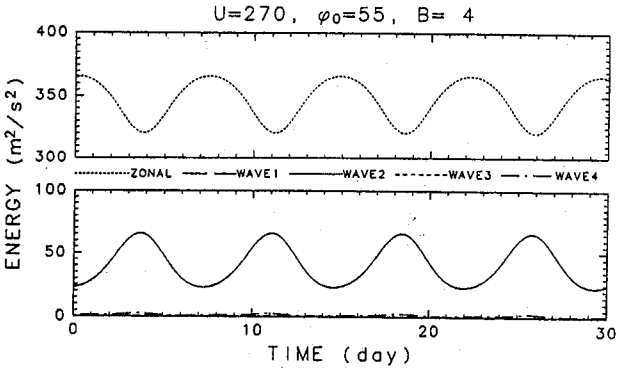


Fig. 2. Evolution of the domain-averaged kinetic energy associated with mean zonal flow and Waves 1, 2, 3, and 4 for a tanh-type jet with $U = 270$ m/s, $B = 4°$, and $\phi_0 = 55°$. The time is measured after a 105-day integration from the initial state when the energy of zonal component has a maximum value.

The initial disturbance is the same one used by IY94; the results are insensitive to the structure of this disturbance. The advection term is computed using a spectral transform method with a triangular truncation of T85 for Eq. (1) and T173 for Eq. (6). The Runge-Kutta-Gill method is used for time-integrations with an increment of 1/150 day.

## 3. Results

### *3.1 The tanh-type jet*

1) dynamical features

Figure 1 is a régime diagram which shows each flow régime as a function of the forcing parameters, $U$, $B$ and $\phi_0$. The symbol $S$ refers to a steady-wave state and $V$ refers to a vacillation in which the wave changes its structure periodically. The lower suffix indicates the dominant zonal wavenumber, and the upper suffix for a steady-wave solution indicates $2\pi/c$ in days, where $c$ is the angular phase velocity of the steady wave. That is, the upper suffix indicates the time needed for the steady wave to travel round the pole. Here, the steady-wave solution of zonal wavenumber 2 is obtained over a wide range of parameters. Such dominance of Wave 2 is consistent with the result in the conserved system obtained by IY94 and the dominance in the parameter space is more remarkable in the present forced-dissipative system. The angular phase velocity of the steady waves, which mainly depends on $U$, is comparable to the observed waves. A steady-wave solution of Wave 3 is obtained for a weak low-latitude jet ($U = 180$ m/s and $\phi_0 = 35°$). The existence of the Wave 3 régime for the low-latitude jet is due to longer parallel of latitudes along the jet axis. Several vacillating solutions are also obtained for the three values of $\phi_0$. However, the nature of the vacillation for $\phi_0 = 35°$ and for $\phi_0 = 45°$ with $B = 8°$ is different from that for $\phi_0 = 45°$ with $B = 4°$ and for $\phi_0 = 55°$. Vacillations for $\phi_0 = 35°$, which appear at the boundary between $S_3$ and $S_2$ régimes, have very slight variation of wave amplitude, and the vacillation for $\phi_0 = 45°$ with $B = 8°$ has the same nature. On the other hand, the vacillations for $\phi_0 = 45°$ with $B = 4°$ and for $\phi = 55°$, which appear when the jet forcing is narrow (small $B$) and intense (large $U$), have a large variation of wave amplitude. Decrease of dominant zonal wavenumber from 3 to 2 along the $U$ axis at $\phi_0 = 35°$ is consistent with the result obtained by Kwon and Mak (1988).

Figure 2 shows an example of the evolution of domain-averaged kinetic energy associated with zonal mean zonal flow and planetary waves (see IY94 for the definition) for the vacillation of $U = 270$ m/s, $B = 4°$, and $\phi_0 = 55°$. The energy is mainly exchanged between the mean zonal flow (dotted line) and Wave 2 (solid line) with a period of 7.36 days. The variation of the wave energy is as much as 50 per cent of the time-mean value. The variation of zonal profiles, $\overline{u}$ and $\overline{q}$, for the vacillating solution is shown in Fig. 3. The negative region of $d\overline{q}/d\phi$ in the initial profile (around $\phi$~50°) almost disappears owing to vorticity mixing by the Wave 2. Corresponding to this change of $\overline{q}$ profile, the jet becomes weak and

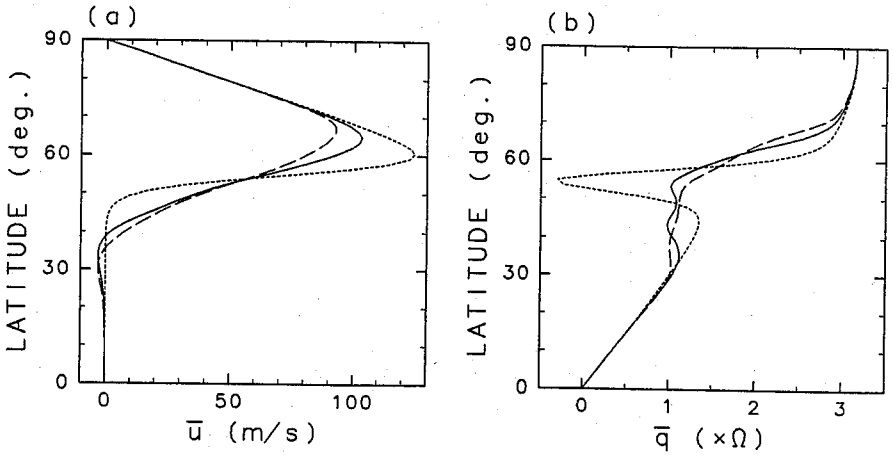


Fig. 3. Variation of the latitudinal profiles of zonal mean zonal wind $\overline{u}(\phi)$ and zonal mean absolute vorticity $\overline{q}(\phi)$ for a tanh-type jet with $U = 270$ m/s, $B = 4°$, and $\phi_0 = 55°$. The dotted line shows the prescribed equilibrium profile (or, the initial state); the solid line and broken line show the profiles at Day 0 and Day 3.68 in Fig. 2, respectively.

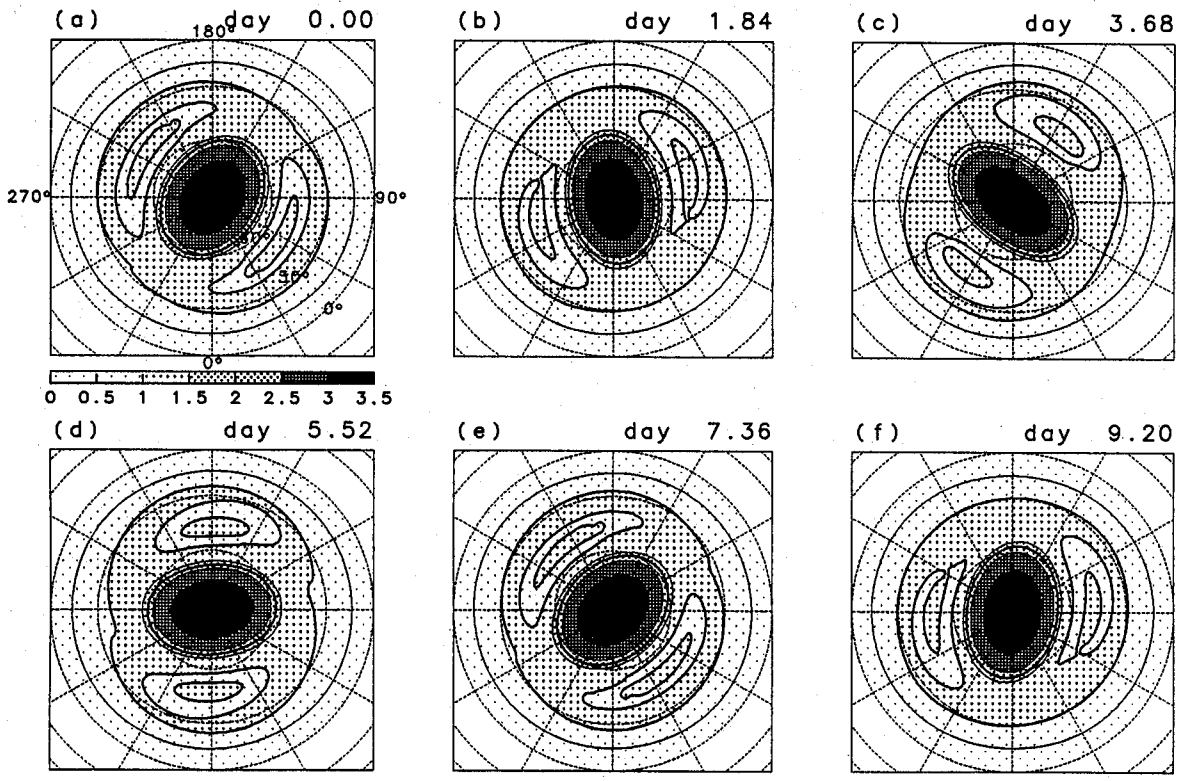


Fig. 4. Evolution of the absolute vorticity ($q$) field for a tanh-type jet with $U = 270$ m/s, $B = 4°$, and $\phi_0 = 55°$ (every quarter of the vacillation cycle is shown). The value is scaled by $\Omega$ and dark shading corresponds to high $q$. Lambert equal area projection is used only for a hemisphere ($\phi \geq 0°$). Meridians and parallels are shown every 30°.

wide. The maximum speed of the jet around $\phi \sim 65°$ fluctuates about 10 per cent in this vacillation cycle. Negative regions of $d\overline{q}/d\phi$ exist in middle latitudes when the zonal flow has a maximum energy (solid line), while they disappear when the wave energy has a maximum (broken line).

Figure 4 shows the evolution of absolute vorticity ($q$) field in the vacillation. The polar vortex changes its shape; stretching (a → c) and shrinking (c → e) in the vacillation cycle. Since the vacillation cycle is 7.36 days, (e) and (f) show the same patterns as (a) and (b), respectively, except for the longitudinal

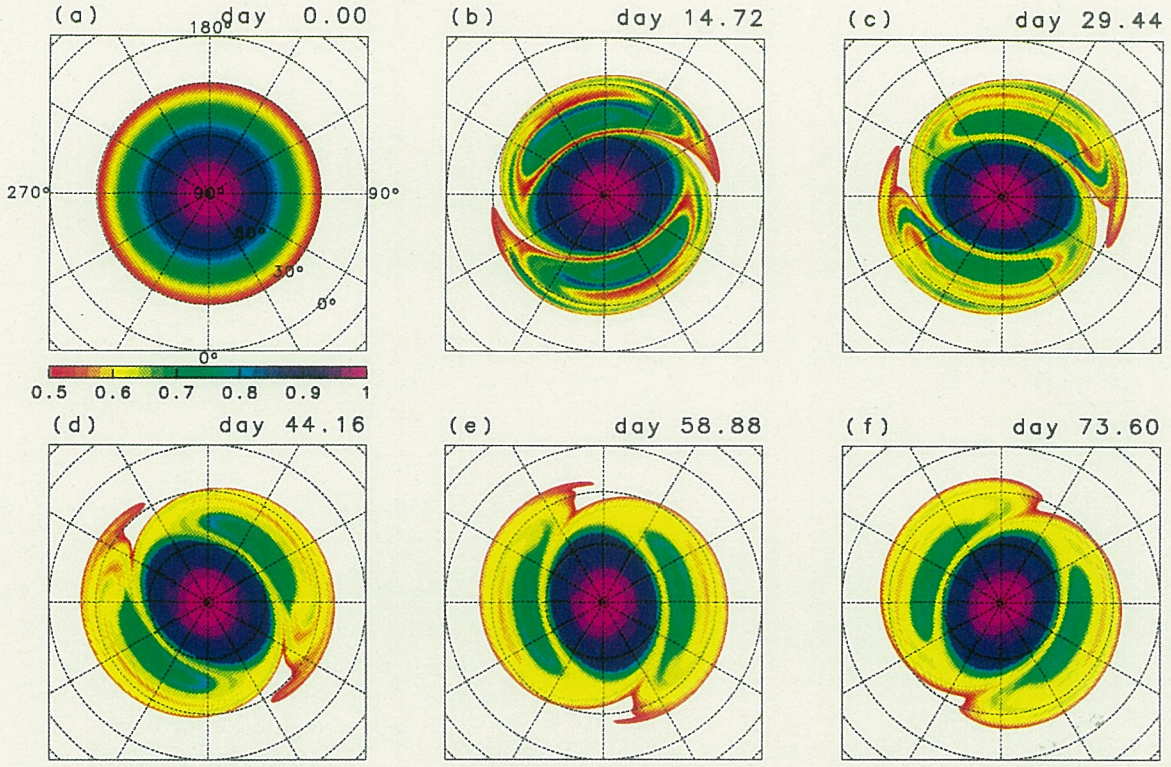


Fig. 5. Evolution of a passive scalar ($\chi$) field for a tanh-type jet with $U = 270$ m/s, $B = 4°$, and $\phi_0 = 55°$ (every two cycles of the vacillation is shown). Each date corresponds to that in Fig. 2.

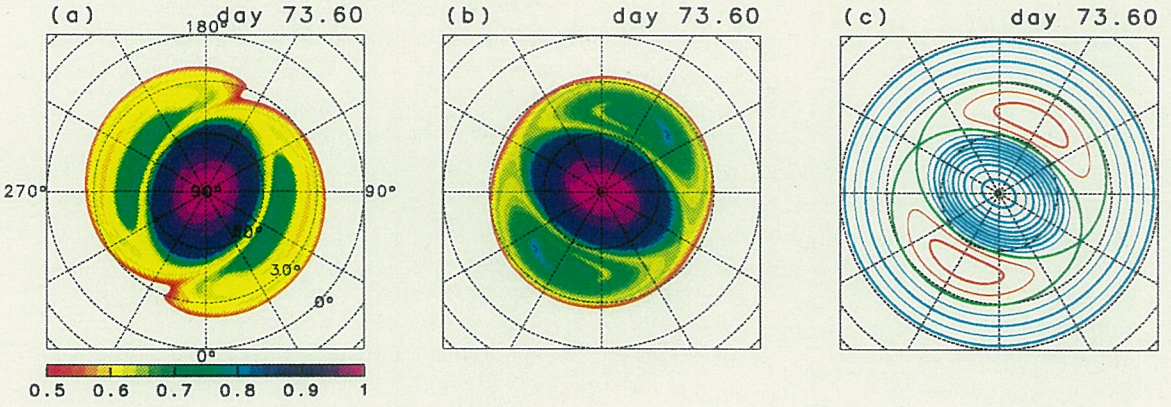


Fig. 6. The passive scalar field after a 73.6 day-integration for a tanh-type jet (a): vacillation with $U = 270$ m/s, $B = 4°$, and $\phi_0 = 55°$, (b): the steady-wave solution with $U = 270$ m/s, $B = 6°$, and $\phi_0 = 55°$. (c): trajectory of a tracer in the same steady-wave solution as (b).

phase. The Wave 2 pattern propagates eastward with an angular phase velocity of $2\pi/16.26$ day$^{-1}$ on average.

2) tracer transport

To investigate tracer transport and mixing processes in the vacillation, Eq. (6) is integrated for 73.6 days (*i.e.*, 10 cycles of the vacillation) from an axisymmetric initial distribution, $\chi = \sin\phi$. Figure 5 shows the evolution of the passive scalar ($\chi$) field over every two cycles of the vacillation. At the early stage of the evolution, thin filaments of fluid are formed and circling around two low-$q$ areas in middle latitudes (b). Then the fluid in middle latitudes is mixed thoroughly through stretching and folding of these filaments (c, d). Finally, the fine structures in middle latitudes are smoothed by the hyper-diffusion and the yellow region spreads (e, f). On the other hand, the fluid inside the polar vortex is isolated from surroundings; in other words, no fluid is exchanged across the vortex boundary

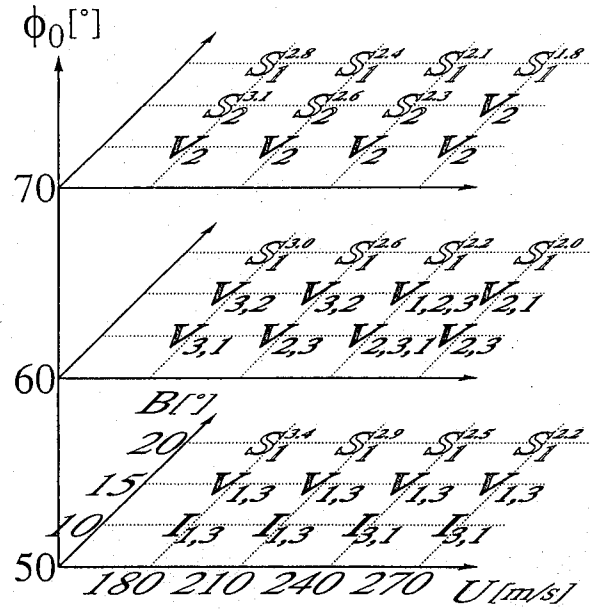


Fig. 7. Same as Fig. 1, except for a sech-type jet. Symbol $I$ refers to an irregularly fluctuating solution.

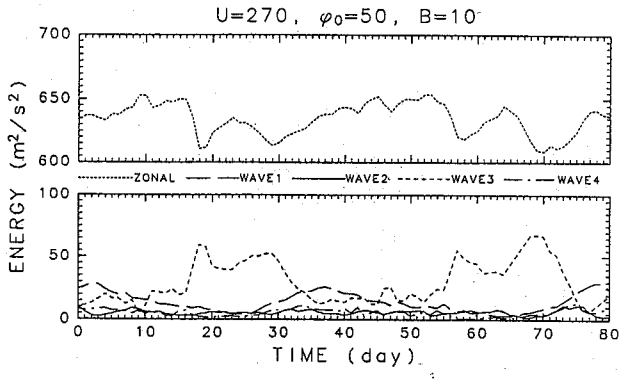


Fig. 8. Same as Fig. 2, except for a sech-type jet with $U = 270$ m/s, $B = 10°$, and $\phi_0 = 50°$. The time is measured after a 100-day integration from the initial state.

around $\phi \sim 60°$.

For the present initial distribution of $\chi$, such a mixing in middle latitudes is not peculiar to vacillating solutions. Figure 6 compares two $\chi$ fields after a 73.6-day integration from the same axisymmetric initial distribution for the vacillation (a) as shown in Fig. 5f and for the steady-wave solution with $U = 270$ m/s, $B = 6°$, and $\phi_0 = 55°$ (b). The mixing in middle latitudes occurs also in the steady-wave solution through shearing rather than stretching and folding. Figure 6c is the streamfunction in the co-moving reference frame with the steady wave shown in (b), which streamfunction gives the particle trajectory (Flierl, 1981; Polvani and Touma, 1992). Heteroclinic orbits connecting two saddle points are drawn by green lines, which separate the anti-cyclonically trapped regions from polar and low-latitude regions. Particles (tracer) inside the trapped regions move eastward in accordance with the eastward-propagating steady wave. Note that fluid in the polar region is also isolated by the heteroclinic orbits. The apparent mixing in Fig. 6b is a transient feature which arose from the choice of the initial distribution of $\chi$; the mixing through shearing continues until the pattern in the passive scalar field corresponds to the trajectory pattern (c). If one chose the streamfunction field shown in Fig. 6c as the initial distribution of the passive scalar, one would not see any subsequent mixing. On the other hand, such a steady trajectory does not exist for the vacillation and "chaotic mixing" (Pierrehumbert, 1991) occurs in the separatrix layers around the heteroclinic orbits. The early stage of the mixing mainly due to shearing is common to steady-wave and vacillating solutions, while the effective mixing indicated by large yellow area as shown in Fig. 5e, 5f is a result of the chaotic mixing in the vacillation.

*3.2 The sech-type jet*

1) dynamical features

The régime diagram for the zonal flow forcing of sech-type jet is shown in Fig. 7. Here, a new symbol $I$ refers to an irregularly fluctuating solution. When $B = 20°$ (wide jets), all the runs fall into steady-wave solutions of zonal wavenumber 1. The angular phase speed of the wave is faster than the observed "4-day wave" because the jet analyzed here is rather intense. For narrower jets, however, an irregular flow régime as well as a vacillation régime exists; stepwise transitions from a steady-wave régime to irregular flow via vacillation take place as $B$ decreases at $\phi_0 = 50°$: The wave field has some dominant zonal wavenumbers in these vacillation and irregular flow, because a negative $d\bar{q}_0/d\phi$ area exists not only in high latitudes but also in middle latitudes for the smaller $B(= 15°, 10°)$ (*cf.* Fig. 9). The interaction between the waves originating from these two unstable regions leads to either vacillation or irregular fluctuation.

Figure 8 shows an example of the evolution of domain-averaged kinetic energy for an irregular solution with $U = 270$ m/s, $B = 10°$, and $\phi_0 = 50°$. The dominant wavenumber is 3 for most of the time, but Wave 1 grows occasionally and Wave 3 decays simultaneously, leading to the dominance of Wave 1 during the periods of Days 0–10, 34–45, and 75–80. Wave 1 is generated in the unstable region in high latitudes while Wave 3 is in middle latitudes. Wave 3, Wave 1 and zonal mean flow interact with one another to cause irregular fluctuation; anti-correlation between zonal mean flow and Wave 3 is evident.

Figure 9 shows variation of the latitudinal profiles

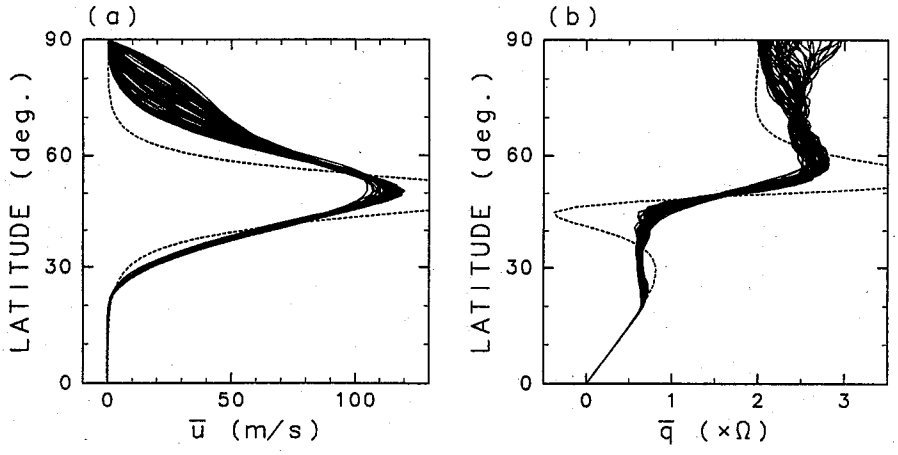


Fig. 9. Same as Fig. 3, except for a sech-type jet with $U = 270$ m/s, $B = 10°$, and $\phi_0 = 50°$. Solid lines show the latitudinal profiles drawn every day from Day 0 to Day 80.

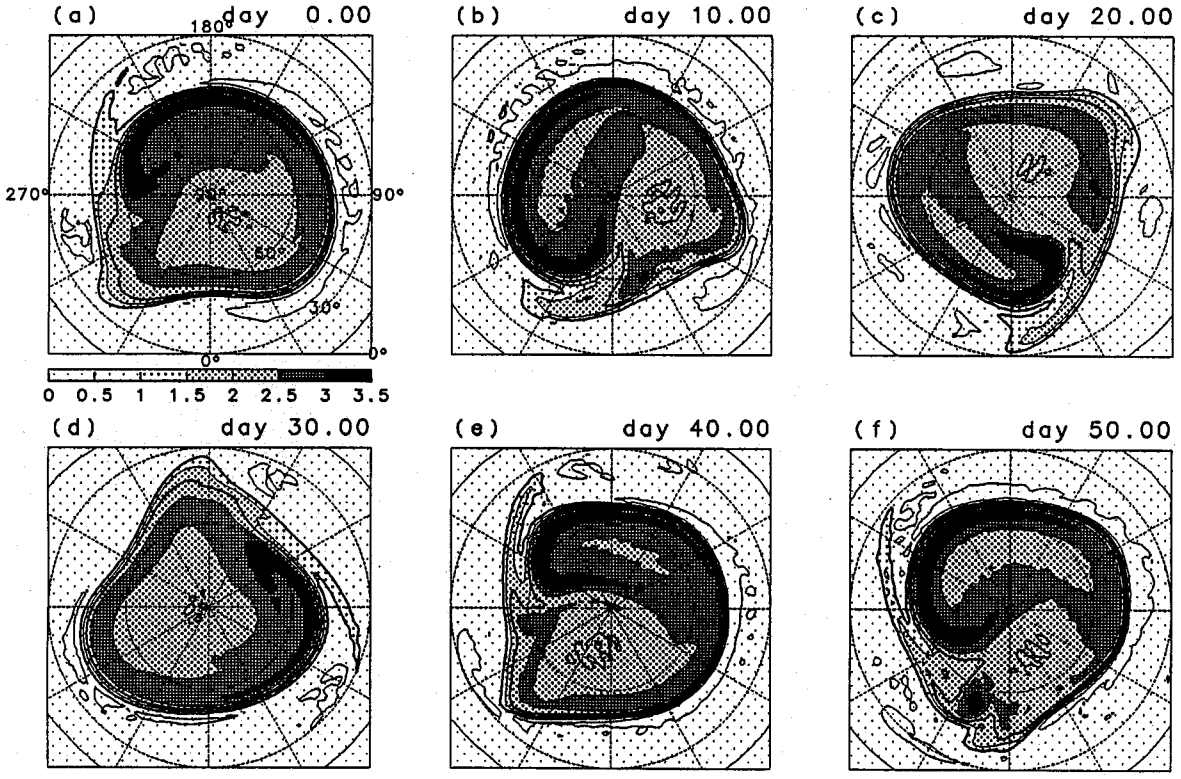


Fig. 10. Same as Fig. 4, except for a sech-type jet with $U = 270$ m/s, $B = 10°$, and $\phi_0 = 50°$. Lambert equal area projection is used for an area of $\phi \geq 30°$.

of $\overline{u}$ and $\overline{q}$ for the irregular solution. Two unstable areas where $d\overline{q}_0/d\phi < 0$ in the prescribed forcing profile (dotted line) exist both in poleward and equatorward flanks of the jet. Momentum transport by the fluctuating waves removes the unstable regions of $d\overline{q}/d\phi < 0$ and makes the jet weak and wide. The zonal mean $\overline{u}$ and $\overline{q}$ fluctuate both in high latitudes and in middle latitudes, but more significantly in high latitudes.

Evolution of the absolute vorticity field for the irregular solution is shown in Fig. 10. The area of highest $q$ does not exist over the pole but is located in a zonal band around $\phi$~60°. Negative gradients of $\overline{q}$ in the polar region shown in Fig. 9 reflect these distributions of $q$. The shape of the polar vortex changes irregularly, reflecting the variation of Wave 1 and Wave 3 shown in Fig. 8. Corresponding to the dominance of Wave 3 between Day 15 and 30, the shape of the polar vortex characterized by sharp gradient of $q$ becomes roughly triangular at Day 30(d).

At Day 40(e), on the other hand, the high-$q$ area has large anti-symmetry about the pole owing to the growth of Wave 1, and the edge of the polar vortex is broken around $\lambda\sim270°$ (a gap of the sharp gradient appears). Note here that a clear boundary to the polar vortex often exists around $\phi\sim50°$.

2) tracer transport

Figure 11 shows the evolution of a passive scalar field for the irregular flow shown in Fig. 10. In middle latitudes around $\phi\sim45°$, the fluid is mixed violently by Wave 3 and others (b, c, d), and eventually the distribution of passive scalar is smoothed out (e, f). Unlike the cases of the tanh-type jet, the fluid inside the polar vortex is also mixed by Wave 1 and others (b–f). Note that a thin filament of fluid in middle latitudes occasionally intrudes deeply into the polar region (the yellow area in (e)) from the broken edge of the polar vortex around $\lambda\sim270°$ (*cf.* Fig. 10e). At the same time a thin filament of polar fluid flows out of the edge. In the greater part of the evolution, the polar fluid is isolated from surroundings and a very sharp gradient of the passive scalar field is maintained at the edge of the polar vortex (around $\phi\sim50°$ in (f)).

Figure 12 shows the passive scalar fields after a 50-day integration from the same axisymmetric distribution as Fig. 11a for three kinds of flow régimes with $U = 270$ m/s and $\phi_0 = 50°$: (a) irregular flow ($B = 10°$), (b) vacillation ($B = 15°$), and (c) steady-wave solution ($B = 20°$). Here, (a) is the same as Fig. 11f. In the vacillation (b), the fluid in middle latitudes is mixed sufficiently and gradients of the passive scalar field is largely smeared out owing to the wave disturbances (dominantly Wave 3) generated by the instability in the equatorward flank of the jet. Inside the polar vortex, the fluid initially in the polar region shown by purple color is shifted to $\phi\sim80°$ by Wave 1 in high latitudes. The chaotic mixing in the vacillation, mainly due to the interaction between the Wave 1 and Wave 3, smooths the passive scalar distribution to some extent (that is, the blue area in (b) spreads), although the vacillation cycle is so long (34 days) that the chaotic mixing is not effective in the 50-day integration. In the steady-wave solution (c), on the other hand, the fluid in middle latitudes is hardly mixed because there is no unstable region in the equatorward flank of the jet. The fluid initially in the polar region is split into two parts by Wave 1; one is the major part centered at $\phi\sim80°$, keeping its initial round shape, and the other is the minor part around $\phi\sim60°$, which shape is a crescent. This pattern of the passive scalar distribution changes little afterward and keeps circling around the pole eastward. The pattern corresponds to the trajectory associated with the steady wave (not shown) as Fig. 6b corresponds to Fig. 6c; the streamfunction in the co-moving frame with the Wave 1 has only one saddle point ($\lambda\sim45°$ and $\phi\sim50°$ at day 50).

## 4. Discussion

We used two types of jet profile introduced by Hartmann (1983) for the zonal flow forcing, sweeping wide parameter ranges which determine the structure of the jet profile. One of the major differences between the régime diagrams obtained for the two types of the jet profiles is the existence of the irregular régime for the sech-type jet. This is because unstable regions can exist in both poleward and equatorward flanks of the sech-type jet. Interactions between the waves originating from these two unstable regions lead to the irregular fluctuations in the flow field. On the other hand, no irregular solution was obtained for the tanh-type jet, which has an unstable region only on the equatorward flank of the jet, even if an unrealistically unstable jet was assumed as intense as $U = 450$ m/s with $B = 4°$ and $\phi_0 = 55°$.

Another significant feature in these régime diagrams is the dominance of Wave 2 for the tanh-type jet, which dominance is more remarkable than that in the conserved system investigated by IY94. It is consistent with the satellite observations that an eastward-propagating Wave 2 is usually dominant in middle latitudes in the southern hemisphere stratosphere during winter and spring (Harwood, 1975; Hartmann, 1976). This correspondence suggests that the eastward-propagating Wave 2 observed by satellites can be caused by the barotropic instability of the circumpolar vortex.

In the analyses of the tracer transport, a common result for both types of jet profile is the robustness of the edge of the polar vortex in resisting exchange of fluid between the inside and outside of the vortex as reported by Bowman and Chen (1994). For the tanh-type jet, there is an unstable region only on the equatorward flank of the jet, so that the fluid is mixed only in middle latitudes. Even if both equatorward and poleward flanks of the jet are unstable for sech-type jet, fluid mixing occurs inside and outside the vortex independently (*e.g.* Fig. 12b). The isolation of the polar vortex is "noticed" in the real atmosphere. The quasi-horizontal transport and mixing properties in and out of the Antarctic polar vortex were investigated by Chen *et al.* (1994) and Chen (1994) with a semi-Lagrangian transport model and a contour advection technique using analyzed winds; in the middle stratosphere the polar vortex is isolated from the midlatitude surf zone in late winter and early spring owing to sharp latitudinal gradients of potential vorticity at the vortex edge, while it is not so isolated in the lower stratosphere.

However, irregular flow for the sech-type jet is an exception: when the jet is so unstable that the edge of the polar vortex is distorted and broken to form

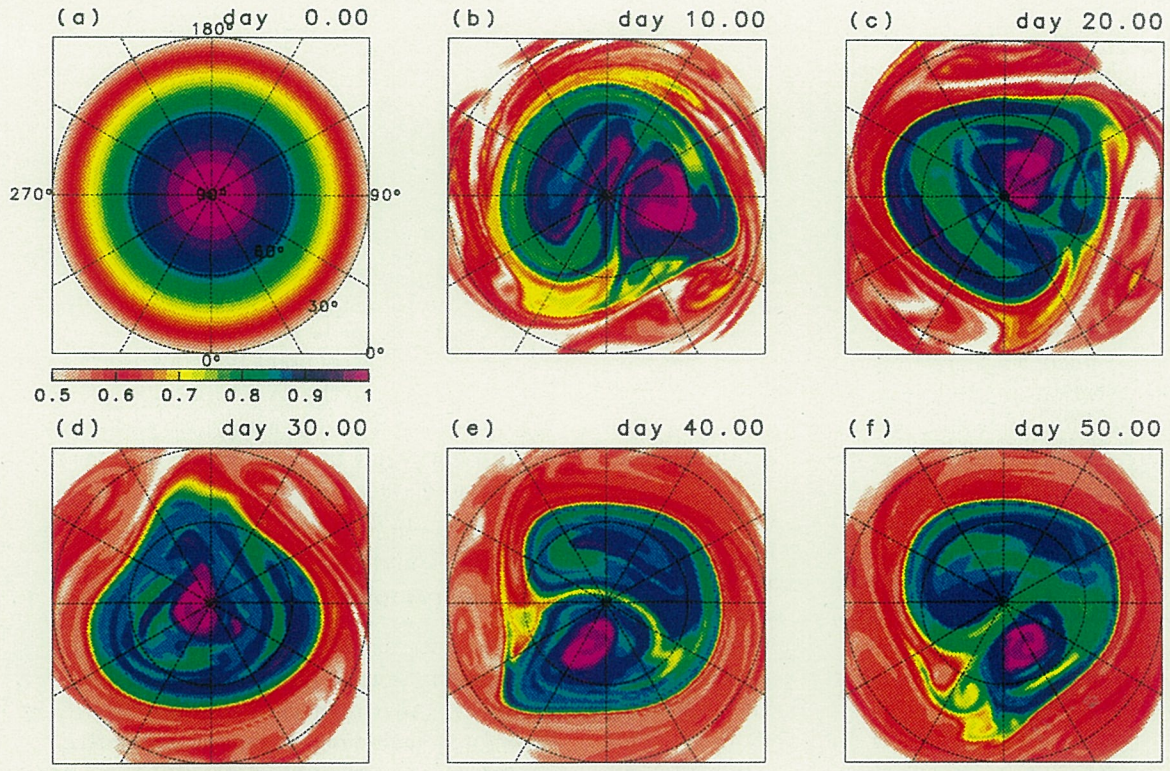


Fig. 11. Same as Fig. 5, except for a sech-type jet with $U = 270$ m/s, $B = 10°$, and $\phi_0 = 50°$. Lambert equal area projection is used only for an area of $\phi \geq 30°$.

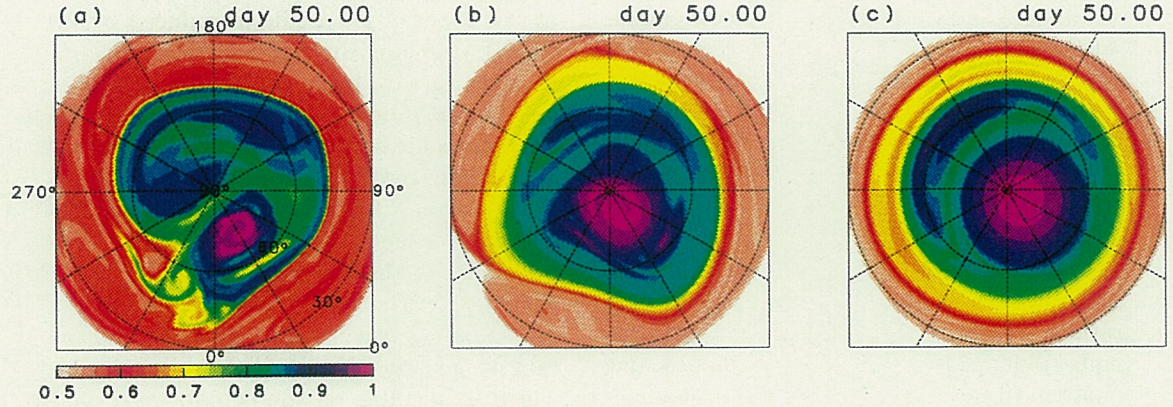


Fig. 12. The passive scalar field after a 50-day integration for sech-type jets with $U = 270$ m/s and $\phi_0 = 50°$. (a): irregular flow with $B = 10°$, (b): vacillation with $B = 15°$, (c): the steady-wave solution with $B = 20°$.

a gap occasionally, fluid outside the vortex intrudes into the vortex while polar fluid inside the vortex is ejected outside in a filamentary structure (*e.g.* Fig. 11e). Similar intrusion and ejection events in the winter stratosphere are observed in LIMS ozone data (Leovy *et al.*, 1985) and in GCM study of Mahlman and Umscheid (1987). Recently, the detail of such a horizontal transport process was investigated using the contour advection technique with analyzed winds (Waugh, *et al.*, 1994; Plumb, *et al.*, 1994) and using a high-resolution numerical model (Norton, 1994). In these studies, intrusion and ejection events occur owing to the breaking of Rossby waves propagating from the troposphere. On the other hand, there is no wave forcing in our model, so that the result of our study proposes another possibility that such intrusion and ejection events can be caused by the instability of the polar vortex alone, although the aforementioned studies have been mainly focused on the middle and lower strato-

sphere while this work might be relevant to the upper stratosphere.

In connection with the contour advection method, we have to comment on the use of hyper-diffusion in our tracer transport model. The use of hyper-diffusion is artificial and inevitable for passive scalar models with grid or spectral methods. The hyper-diffusion smooths fine structures close to the grid scale selectively and gives a kind of coarsely averaged view (in the T173 truncation, $\Delta\lambda\sim0.7°$). Then, the area smoothed by the hyper-diffusion must be filled with very fine structures if the contour advection method is used. However, the effect of hyper-diffusion would be justified if sub-grid scale mixing processes take place owing to local shear and/or convective instabilities which might be associated with gravity waves propagating in the stratosphere.

Pierrehumbert (1991) did pioneering work on the chaotic mixing in a geophysical fluid, mainly with a kinematic study. We showed an example of the chaotic mixing in vacillation (quasi-periodic flow field) by comparing with the mixing due to shearing in a steady-wave solution (periodic flow field). This is the first attempt to get a dynamically consistent simulation of the chaotic mixing in a quasi-periodic flow field. On the other hand, previous studies on the Rossby wave breaking have shown examples of irreversible mixing in an irregular non-periodic flow field (*e.g.*, Juckes and McIntyre, 1987). A common feature of these mixing processes is the importance of the saddle point in the co-moving frame with a steady wave (Fig. 6c), or the stagnation point used in the kinematic analysis by Polvani and Plumb (1992). These points are defined as points where flow speed is identical to the phase velocity of the wave. For the case of forced waves, the points are located in the critical layer, in which irreversible mixing occurs dominantly as reported for several flow configurations (Juckes and McIntyre, 1987; Polvani and Plumb, 1992; Bowman, 1993; Nakamura and Plumb, 1994). In our study, the existence of the saddle point in the steady-solution is essential to the chaotic mixing in the separatrix layers shown in Figs. 5 and 6. The kinematics of particle motions around this point is common to these mixing processes, whether the flow field is quasi-periodic or chaotic.

While the studies cited above investigated several aspects of the transport processes by numerical means, relevant laboratory experiments were conducted by Sommeria, Meyers and Swinney (1989). They produced barotropically unstable jets by pumping fluid in a rotating annular tank with a sloping bottom and investigated tracer transport associated with waves generated by the barotropic instability by injecting dye into the fluid. They showed that the jet acts as a barrier to tracer transport and observed filamentary intrusion and ejection of fluid, which is consistent with our results. However, the intrusion is not so dramatic as we observed in the irregular solution for the sech-type jet because of the annular geometry that suppresses the flow toward the vortex center.

Finally, another correspondence of the results with the real atmosphere is a coherent blob of absolute vorticity circling eastward around the pole obtained for the sech-type jet (it is not shown, but its structure is similar to the passive scalar field shown in Fig. 12c). This coherent blob of absolute vorticity may correspond to the "warm pool" circling the pole with a period of nearly 4 days, which is reported by Prata (1984) and Lait and Stanford (1988). It will be an interesting subject to analize the dynamical features of the stratosphere during the periods when the warm pool is observed.

## 5. Conclusions

Non-linear aspects of a barotropically unstable circumpolar vortex in a forced-dissipative system are investigated numerically with a high-resolution barotropic model on a spherical domain. Linear relaxation to a prescribed zonal jet, of which the meridional profile satisfies the instability condition, is assumed with a plausible value of the relaxation time in the stratosphere. To investigate the flow régimes, thirty six experiments are done for each of two types of jet profile introduced by Hartmann (1983), changing three parameters which determine the structure of the jet profile. Horizontal transport and mixing processes of a passive scalar are also investigated for several types of evolving flow fields with a high-resolution transport model.

Vacillating and irregular solutions are obtained within some parameter ranges as well as steady wave solutions. In the vacillation, planetary waves propagate eastward, changing the horizontal structure periodically. Wave-zonal flow interaction is important to generate the vacillation in a tanh-type jet which is unstable on the equatorward flank of the jet, while wave-wave interactions are also important for a sech-type jet which is unstable mainly on the poleward flank of the jet. Stepwise transitions from steady wave solutions to irregular ones via vacillations are found for the sech-type jet, while no irregular solutions are obtained for the tanh-type jet. A steady-wave or vacillation régime of zonal wavenumber 2 is dominant for the tanh-type jet within realistic parameter ranges of the stratosphere.

Time evolutions of an ideal passive tracer field show that in vacillating and irregular solutions the fluid is mixed through stretching and folding of fluid as well as shearing in a steady-wave solution. Large-scale mixing takes place in middle latitudes for the tanh-type jet, while the fluid initially in the polar region is advected off the pole for the sech-type jet.

Since the mixing occurs inside or outside of the vortex independently, the mixing through the edge of the vortex hardly occurs for either type of jet profile. For the sech-type jet, however, intermittent intrusion and ejection of fluid in a filament structure can occur through the vortex edge, when the vortex is so unstable that the flow fluctuates irregularly.

## Acknowledgments

The authors thank Ping Chen, Jim Holton, and an anonymous reviewer for their very constructive comments on the original manuscript. The GFD-DENNOU Library was used for drawing the figures. K. Ishioka is supported by JSPS Fellowships for Japanese Junior Scientists and this work was supported in part by the Grant-in-Aid for Scientific Research, the Ministry of Education, Science, and Culture of Japan, and by the Grant-in-Aid for the Cooperative Research with Center for Climate System Research, University of Tokyo.

## References

Bowman, K.P., 1993: Barotropic simulation of large-scale mixing in the antarctic polar vortex. *J. Atmos. Sci.*, **50**, 2901–2914.

Bowman, K.P. and P. Chen, 1994: Mixing by barotropic instability in a nonlinear model. *J. Atmos. Sci.*, accepted.

Chen, P., 1994: The permeability of the Antarctic vortex edge. *J. Geophys. Res.*, **99**, 20563–20571.

Chen, P., J.R. Holton, A. O'Neil and R. Swinbank, 1994: Quasi-horizontal transport and mixing in the Antarctic stratosphere. *J. Geophys. Res.*, **99**, 16851–16866.

Flierl, G.R., 1981: Particle motions in large-amplitude wave fields. *Geophys. Astrophys. Fluid Dynamics*, **18**, 39–74.

Hartmann, D.L., 1976: The structure of the stratosphere in the southern hemisphere during late winter 1973 as observed by satellite. *J. Atmos. Sci.*, **33**, 1141–1154.

Hartmann, D.L., 1983: Barotropic instability of the polar night jet stream. *J. Atmos. Sci.*, **40**, 817–835.

Harwood, R.S., 1975: The temperature structure of the southern hemisphere stratosphere August-October 1971. *Quart. J. R. Meteor. Soc.*, **101**, 75–91.

Ishioka, K. and S. Yoden, 1994: Non-linear evolution of a barotropically unstable circumpolar vortex. *J. Meteor. Soc. Japan*, **72**, 63–80.

Juckes, M.N. and M.E. McIntyre, 1987: A high-resolution one-layer model of breaking planetary waves in the stratosphere. *Nature*, **328**, 590–596.

Kwon, H.J. and M. Mak, 1988: On the equilibration in nonlinear barotropic instability. *J. Atmos. Sci.*, **45**, 294–308.

Lait, L.R. and J.L. Stanford, 1988: Fast, long-lived features in the polar stratosphere. *J. Atmos. Sci.*, **45**, 3800–3809.

Leovy, C.B., C-R. Sun, M.H. Hitchman, E.E. Remsberg, J.M. Russell, III, L.L. Gordley, J.C. Gille and L.V. Lyjak, 1985: Transport of ozone in the middle stratosphere: evidence for planetary wave breaking. *J. Atmos. Sci.*, **42**, 230–244.

Mahlman, J.D. and L.J. Umscheid, 1987: Comprehensive modeling of the middle atmosphere: the influence of horizontal resolution. *Transport Processes in the Middle Atmosphere*, G. Visconti and R. Garcia, Ed. D. Reidel Publishing Company, 251–266.

Manney, G.L., 1991: The stratospheric 4-day wave in NMC data. *J. Atmos. Sci.*, **48**, 1798–1811.

Manney, G.L., J.D. Farrara and C.R. Mechoso, 1991: The behavior of wave 2 in the southern hemisphere stratosphere during late winter and early spring. *J. Atmos. Sci.*, **48**, 976–998.

Manney, G.L., C.R. Mechoso, L.S. Elson and J.D. Farrara, 1991: Planetary-scale waves in the southern hemisphere winter and early spring stratosphere: stability analysis. *J. Atmos. Sci.*, **48**, 2509–2523.

Manney, G.L., T.R. Nathan and J.L. Stanford, 1988: Barotropic stability of realistic stratospheric jets. *J. Atmos. Sci.*, **45**, 2545–2555.

Manney, G.L. and W.J. Randel, 1993: Instability at the winter stratopause: A mechanism for the 4-day wave. *J. Atmos. Sci.*, **50**, 3928–3938.

McIntyre, M.E., 1989: On the antarctic ozone hole. *J. Atmos. Terr. Phys.*, **51**, 29–43.

Nakamura, M. and R.A. Plumb, 1994: The effects of flow asymmetry on the direction of Rossby wave breaking. *J. Atmos. Sci.*, **51**, 2031–2045.

Norton, W.A., 1994: Breaking Rossby waves in a model stratosphere diagnosed by a vortex-following coordinate system and a technique for advecting material contours. *J. Atmos. Sci.*, **51**, 654–673.

Pierrehumbert, R.T., 1991: Chaotic mixing of tracer and vorticity by modulated travelling Rossby waves. *Geophys. Astrophys. Fluid Dynamics*, **58**, 285–319.

Plumb, R.A., D.W. Waugh, R.J. Atkinson, P.A. Newman, L.R. Lait, M.R. Schoeberl, E.V. Browell, A.J. Simmons and M. Loewenstein, 1994: Intrusions into the lower stratospheric arctic vortex during the winter of 1991–1992. *J. Geophys. Res.*, **99**, 1089–1105.

Polvani, L.M. and R.A. Plumb, 1992: Rossby wave breaking, microbreaking, filamentation, and secondary vortex formation: The dynamics of a perturbed vortex. *J. Atmos. Sci.*, **49**, 462–476.

Polvani, L.M. and J. Touma, 1992: A note on recent experiments with Rossby waves on eastward jets. *Nonlinear phenomena in atmospheric and ocean physics*, G.F. Carnevale and R.T. Pierrehumbert, Ed. Springer Verlag, 177–185.

Prata, A.J., 1984: The 4-day wave. *J. Atmos. Sci.*, **41**, 150–155.

Sommeria, J., S.D. Meyers and H.L. Swinney, 1989: Laboratory model of a planetary eastward jet. *Nature*, **337**, 58–61.

Venne, D. and J. Stanford, 1979: Observation of a 4-day temperature wave in the polar winter stratosphere. *J. Atmos. Sci.*, **36**, 2016–2019.

Venne, D. and J. Stanford, 1982: An observational study of high-latitude stratospheric planetary waves in the winter. *J. Atmos. Sci.*, **39**, 1026–1034.

Waugh, D.W., R.A. Plumb, R.J. Atkinson, M.R. Schoeberl, L.R. Lait, P.A. Newman, M. Loewenstein, D.W. Toohey, L.M. Avallone, C.R. Webster and R.D. May, 1994: Transport out of the lower stratospheric arctic vortex by Rossby wave breaking. *J. Geophys. Res.*, **99**, 1071–1088.

# 強制-散逸系における順圧不安定な極渦の非線形な様相: 流れ場のレジームと物質輸送

**石岡圭一・余田成男**
(京都大学理学部地球物理学教室)

強制と散逸のある、球面上の高分解能2次元非発散モデルにおいて、極渦の順圧不安定に関する非線形数値実験を行った。また、いくつかの流れ場について、高分解能の輸送モデルを用いて、トレーサーの水平輸送および混合過程を調べた。

帯状ジェット強制のパラメータに依存して、定常な東進ロスビー波 (周期解)、東進波が周期変化するバシレーション (準周期解)、および非周期変動 (カオス解) が得られた。sech 型ジェット (主にジェットの極側が不安定) では定常波解からバシレーションを経由して非周期変動に至る段階的な遷移が見られたが、tanh 型ジェット (ジェットの赤道側が不安定) では現実的パラメター範囲では非周期変動は得られなかった。

また、輸送モデルを用いた実験の結果、波動解が定常であるか非定常であるかに関わらず、極渦の周縁は非常に頑丈で、極渦の内外の流体同士の混合はほとんど起らないことが示された。ただし、sech 型ジェットで得られた非周期変動においては、時折、極渦の内外の流体がフィラメント的な形状をとって交換される。